Article

pubs.acs.org/Biomac

Vitamin E-Oligo(methyl diglycol L-glutamate) as a Biocompatible and Functional Surfactant for Facile Preparation of Active Tumor-Targeting PLGA Nanoparticles

Jintian Wu, Jian Zhang, Chao Deng,* Fenghua Meng, and Zhiyuan Zhong*

Biomedical Polymers Laboratory, and Jiangsu Key Laboratory of Advanced Functional Polymer Design and Application, College of Chemistry, Chemical Engineering and Materials Science, Soochow University, Suzhou 215123, People's Republic of China

Supporting Information

ABSTRACT: Poly(D,L-lactide-*co*-glycolide) (PLGA) nanoparticles have attracted an enormous interest for controlled drug delivery. Their clinical applications are, however, partly hindered by lack of biocompatible, biodegradable and functional surfactants. Here, we designed and developed a novel biocompatible surfactant based on amphiphilic vitamin E-oligo(methyl diglycol L-glutamate) (VEOEG) for facile fabrication of robust and tumor-targeting PLGA-based nanomedicines. VEOEG was prepared with controlled M_n of 1.7−2.6 kg/mol and low molecular weight distribution ($Đ$ = 1.04−1.16) via polymerization of methyl diglycol L-glutamate *N*-carboxyanhydride using vitamin E-ethylenediamine derivative (VE-NH_2) as an initiator. VEOEG had a hydrophile−lipophile balance data of 13.8−16.1 and critical micellar concentration of 189.3−203.8 mg/L depending on lengths of oligopeptide. Using VEOEG as a surfactant, PLGA nanoparticles could be obtained via nanoprecipitation method with a small and uniform hydrodynamic size of 135 nm and positive surface charge of +26.6 mV, in accordance with presence of amino groups at the surface. The resulting PLGA nanoparticles could be readily coated with hyaluronic acid (HA) to form highly stable, small-sized (143 nm), monodisperse, and negatively charged nanoparticles (HA-PLGA NPs). Notably, paclitaxel-loaded HA-PLGA NPs (PTX-HA-PLGA NPs) exhibited better antitumor effects in CD44-positive MCF-7 breast tumor cells than Taxol (a clinical paclitaxel formulation). The in vivo pharmacokinetics assay in nude mice displayed that PTX-HA-PLGA NPs possessed a long plasma half-life of 3.14 h. The in vivo biodistribution studies revealed that PTX-HA-PLGA NPs had a high tumor PTX level of 8.4% ID/g, about 6 times better than that of Taxol. Interestingly, therapeutic studies showed that PTX-HA-PLGA NPs caused significantly more effective tumor growth inhibition, better survival rate and lower adverse effect than Taxol. VEOEG has emerged as a versatile and functional surfactant for the fabrication of advanced anticancer nanomedicines.

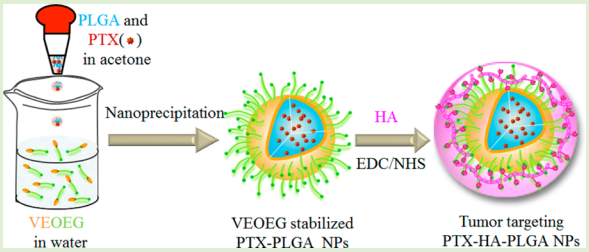

1. INTRODUCTION

Biodegradable nanoparticles and microparticles based on poly(D,L-lactide-*co*-glycolide) (PLGA) are undoubtedly one of the most important platforms to achieve targeted or sustained delivery of varying therapeutic agents.[1−6] For example, several protein and peptide-loaded PLGA microparticles like Lupron Depot, Decapeptyl, Somatuline LA, and Nutropin Depot have come to the market for the treatment of prostate cancer, acromegaly, and growth hormone deficiency.[7,8] PLGA nano/microparticles are typically prepared by emulsion solvent evaporation technique and nanoprecipitation method, which require surfactants to stabilize the dispersed droplets, reduce their surface tension, and inhibit coalescence.[9] Because of their high viscosity in aqueous solution and strong adsorption around the suspension droplets, poly(vinyl alcohol), poloxamer, and poly(vinylpyrrolidone) are the most commonly applied to fabricate uniform PLGA microspheres and nanoparticles for controlled delivery of various proteins and drugs.[10,11] These macromolecular surfactants are, however, associated with several drawbacks such as nonbiodegradability, potential toxicity, and lack of functional groups.[12]

Vitamin E polyethylene glycol-succinate (TPGS) has recently appeared as a versatile and biocompatible surfactant.[13] Feng and Mu reported that TPGS could be applied for the preparation of 300−800 nm PLGA nanoparticles (PLGA NPs), and exhibited higher emulsification effects and improved loading efficiency compared with PVA.[14,15] TPGS has shown to inhibit drug efflux, thus enhancing the cytotoxicities of anticancer drugs like doxorubicin, docetaxel, and PTX in multidrug resistant cancer cells.[16−18] Moreover, TPGS showed intrinsic anticancer activities and could inhibit the growth of human lung tumor in nude mice.[19] PLGA micro/nanoparticles stabilized by TPGS have, however, generally low stability and difficulty in surface functionalization with bioactive molecules.

Here, we report on a novel class of biocompatible and functional surfactants based on vitamin E-oligo(methyl diglycol L-glutamate) and their application for facile preparation of multifunctional PLGA NPs for active tumor-targeting paclitaxel

Received: March 13, 2016
Revised: June 12, 2016
Published: June 15, 2016

DOI: 10.1021/acs.biomac.6b00380
Biomacromolecules 2016, 17, 2367−2374

(PTX) delivery in vivo (Scheme 1). Vitamin E-oligopeptide can be readily prepared by polymerization of methyl diglycol L-glutamate *N*-carboxyanhydride (EG_2-Glu-NCA) using vitamin E-ethylenediamine derivative (VE-NH_2) as an initiator. Oligopeptide have generally excellent biocompatibility and biodegradability to nontoxic products in vivo. Polypeptides are widely explored for drug delivery and regenerative medicine.[20−27] Vitamin E is a well-known natural antioxidant and its derivatives have been reported to enhance therapeutic delivery.[28,29] It should be noted that the hydrophobic vitamin E head portion and hydrophilic oligopeptide tail are bulky and have large surface areas, which is an essential characteristic of a good surfactant. The terminal amino groups of VEOEG surfactants following preparation of nanoparticles via nanoprecipitation would locate on the surface of PLGA NPs, and facilitate both shell-cross-linking and ligand decoration with biomolecules like polysaccharides, peptides, and antibodies, affording robust and multifunctional PLGA NPs for active tumor-targeting chemotherapy.

Scheme 1. Preparation of PTX-Loaded HA-PLGA NPs (PTX-HA-PLGA NPs) by Nanoprecipitation Method Using VEOEG as a Novel Functional Surfactant Followed by HA Coating for Active Tumor-Targeting Delivery of PTX

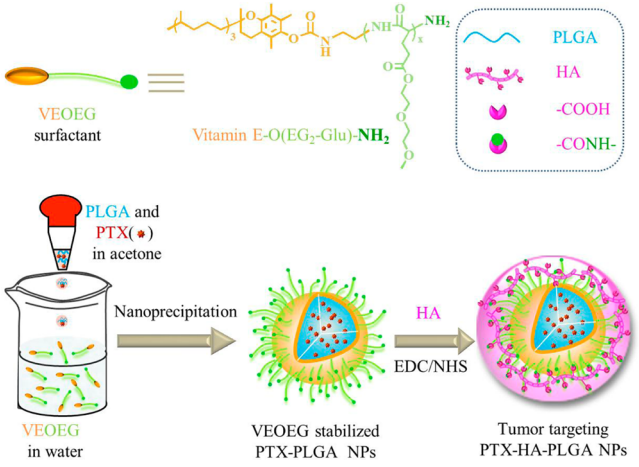

2. EXPERIMENTAL METHODS

2.1. Synthesis of Vitamin E-NH_2. Briefly, 4-nitrophenyl chloroformate (4-NC) (1.98 g, 9.8 mmol) in DCM (30 mL) was dropwise added to DCM (10 mL) solution of vitamin E (VE) (2.12 g, 4.9 mmol) and pyridine (1.98 mL, 24.5 mmol) under nitrogen atmosphere at 0 °C. The reaction proceeded at 30 °C overnight. The mixture was filtered to remove the pyridine hydrochloride, and then evaporated to remove DCM to obtain raw product. The product was purified by dissolving in petroleum ether (b.p: 60−90 °C) and removing the insolubles by centrifugation at −5 °C. The evaporation of the solvent yielded Vitamin E-4-NC as a yellowish oil. Yield: 93.4%. ^{1}H NMR (400 MHz, $CDCl_3$, Figure S1A): δ 8.32, 8.30, 7.49,7.46 (d, $NO_2-C_6\mathbf{H}_4-$); 2.62 (t, $-Ph(CH_3)_3C\mathbf{H}_2CH_2-$); 2.16, 2.12 (s, $-Ph(C\mathbf{H}_3)_3-$); 1.80 (t, $-Ph(CH_3)_3CH_2C\mathbf{H}_2-$); 1.57 (m, $CH_3(C\mathbf{H}(CH_3)CH_2CH_2CH_2)_3-$); 1.38−1.07 (m, $CH_3(CH(CH_3)-\mathbf{CH}_2\mathbf{CH}_2\mathbf{CH}_2)_3-$; s, $-C(\mathbf{CH}_3)O-$); 0.87−0.83 (d, $\mathbf{CH}_3(CH(\mathbf{CH}_3)-CH_2CH_2CH_2)_3-$).

To a solution of ethylenediamine (1.35 mL, 20 mmol) and pyridine (1.6 mL, 20 mmol) in DCM (4 mL), VE-4-NC (0.6 g, 1.0 mmol) solution in DCM (14 mL) was added dropwise under a N_2 atmosphere. The reaction proceeded overnight at room temperature (r.t.). The reaction mixture was washed with distilled water until the water phase became colorless. The DCM solution was dried with anhydrous magnesium sulfate at −24 °C for 24 h. The solution was filtered and the filtrate was evaporated. Yield: 78.1%. ^{1}H NMR (400 MHz, $CDCl_3$, Figure S1B): δ 3.33 (t, $-NHC\mathbf{H}_2CH_2NH_2$); 2.90 (t, $-NHCH_2C\mathbf{H}_2NH_2$); 2.58 (t, $-Ph(CH_3)_3C\mathbf{H}_2CH_2-$); 2.08, 2.02 (s, $-Ph(C\mathbf{H}_3)_3-$); 1.77 (t, $-Ph(CH_3)_3CH_2C\mathbf{H}_2-$); 1.52 (m, $CH_3(C\mathbf{H}(CH_3)CH_2CH_2CH_2)_3-$); 1.37−1.07 (m, $CH_3(CH(CH_3)-\mathbf{CH}_2\mathbf{CH}_2\mathbf{CH}_2)_3-$; s, $-C(\mathbf{CH}_3)O-$); 0.87−0.83 (d, $\mathbf{CH}_3(CH(\mathbf{CH}_3)-CH_2CH_2CH_2)_3-$).

2.2. Synthesis of Vitamin E-O(EG_2-Glu) (VEOEG). VEOEG was synthesized by polymerization of EG_2-Glu-NCA with VE-NH_2 as an initiator. The following is a typical example on synthesis of $VEOEG_5$ (5 denoted as the degree of polymerization of EG_2-Glu). Under a N_2 atmosphere, a DCM solution (37 mL) of VE-NH_2 (1.16 g, 2.25 mmol) was quickly added into a DCM solution (37 mL) of EG_2-Glu-NCA (3.71 g, 13.50 mmol). The reaction mixture was stirred for 12 h at 25 °C, condensed to about 18 mL, and then precipitated in diethyl ether. The product was dried at r.t. in vacuum for 24 h. Yield: 55.8%. ^{1}H NMR (600 MHz, $CDCl_3$, Figure 1A): δ 4.24 (m, $-NHCOC\mathbf{H}-$; t, $CH_3OCH_2CH_2OCH_2C\mathbf{H}_2-$); 3.68−3.54 (m, $CH_3OCH_2\mathbf{CH}_2OCH_2CH_2-$); 3.40−3.36 (t, $-NHC\mathbf{H}_2CH_2NH-$; s, $C\mathbf{H}_3OCH_2CH_2OCH_2CH_2-$); 2.66−2.34 (t, $-Ph(CH_3)_3C\mathbf{H}_2CH_2-$, t, $-COCH(NH)CH_2C\mathbf{H}_2-$); 2.07, 2.03 (s, $-Ph(C\mathbf{H}_3)_3-$); 1.99−1.88 (m, $-COCH(NH)C\mathbf{H}_2CH_2-$); 1.78 (t, $-Ph(CH_3)_3CH_2C\mathbf{H}_2-$); 1.53 (m, $CH_3(C\mathbf{H}(CH_3)CH_2CH_2\ CH_2)_3-$); 1.37−1.07 (m, $CH_3(CH-(CH_3)C\mathbf{H}_2\mathbf{CH}_2\mathbf{CH}_2)_3-$; s, $-C(\mathbf{CH}_3)\ (CH_2)-$); 0.87−0.83 (d, $\mathbf{CH}_3(CH(\mathbf{CH}_3)CH_2CH_2CH_2)_3-$). MALDI-TOF showed an M_n of 1695.1, which was in accordance with a degree of polymerization of 5. The amount of amino groups at the chain end of VEOEG was determined by TNBSA assay.

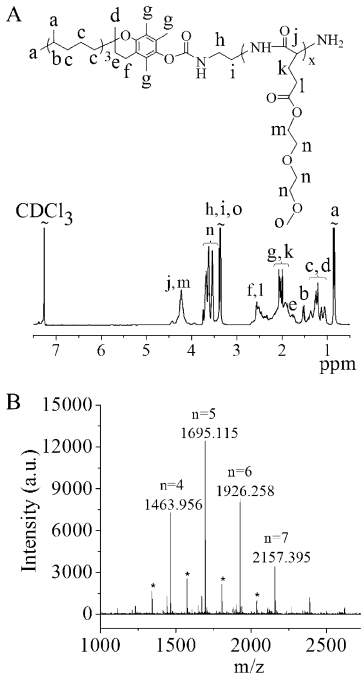

Figure 1. ^{1}H NMR spectrum (600 M Hz, $CDCl_3$) (A) and MALDI-TOF spectrum (B) of vitamin E-O(EG_2-Glu)$_5$. $m/z = M_n + Na^+ = 516.4 + 231.1 \times n + 23.0$. Asterisk (*) denotes products with backbiting.

The critical micelle concentration (CMC) of VEOEG was measured with pyrene (0.6 μM) as a fluorescent probe. VEOEG had varying concentrations from 0.2 to 2000 mg/L. The fluorescence spectra were obtained using Cary Eclipse fluorescence spectrophotometer (Agilent Technologies, excitation wavelength: 330 nm). The CMC was determined as the cross-point when extrapolating the intensity rate I_{383}/I_{372} at high and low concentration regions.

DOI: 10.1021/acs.biomac.6b00380
Biomacromolecules 2016, 17, 2367−2374

2.3. Fabrication of PLGA NPs. PLGA NPs were prepared using VEOEG as a surfactant by nanoprecipitation method.[30] Briefly, 0.9 mL of PLGA solution in acetone (10.0 mg/mL) was added dropwise to 9.0 mL of VEOEG aqueous solution (0.45 mg/mL) under stirring at rt. After stirring for 6 h, the acetone was evaporated. The resulting sample was collected by centrifugation (12 000 rpm, 10 min, 4 °C; Sorvall Biofuge Stratos, Thermo Scientific) and washed once with deionized water. The amount of VEOEG located on the surface of PLGA NPs was determined by comparing the integrals of OEG methylene protons at δ 3.54−3.68 with methine proton of PLGA at δ 5.21 (Figure S2).

2.4. Preparation of Hyaluronic Acid Coated PLGA NPs (HA-PLGA NPs). HA-PLGA NPs were formed through coating positively charged PLGA NPs with negatively charged HA followed by coupling reaction using EDC/NHS as coupling agents. Briefly, HA (45.5 mg, 1.3 μmol, 120.0 μmol carboxyl groups) was dissolved in 4.0 mL of acetate buffer (0.1 M, pH 5.0) and preactivated using EDC (6.9 mg, 36.0 μmol) and NHS (2.1 mg, 18.0 μmol) for 0.5 h at rt. The activated HA was added to the PLGA NPs suspension (VEOEG/activated carboxyl = 3:1 mol/mol) in $NaCO_3/NaHCO_3$ buffer (pH 9.0) followed by incubation overnight at 37 °C to form HA-PLGA NPs. Excess reactive agents and byproducts were removed by extensive dialysis (MWCO 350 000 Da) against deionized water.

2.5. Drug Loading. PTX was loaded into nanoparticles through dropwise addition of acetone solution of PTX and PLGA (theoretical drug loading content: 8 wt %) to water phase containing a predetermined amount of VEOEG under stirring at room temperature. PTX-loaded PLGA NPs (PTX−PLGA NPs) were coated with HA as described above.

Drug loading content (DLC) and drug loading efficiency (DLE) were measured by high performance liquid chromatography (HPLC, Agilent Technologies 1260 Infinity) equipped with a reverse-phase HPLC column (Sepax GP-C18, 4.6 × 150 mm, 5 μm). Briefly, 200 μL of PTX-loaded HA-PLGA NPs (PTX-HA-PLGA NPs) were freeze-dried, dissolved in acetonitrile/water (1:1, v/v) solution, and filtered through 0.45 μm filter. The drug was detected with UV at 227 nm. The acetonitrile/water solvent mixture was used as a mobile phase, the flow rate was fixed at 1.0 mL/min, and the standard curve was obtained at different PTX concentrations (0.05−100 μg/mL). DLC and DLE were calculated according to the following formula:

$$\mathrm{DLC(wt\ \%)} = \frac{\text{weight of loaded drug}}{\text{total weight of loaded drug and polymer}} \times 100$$

$$\mathrm{DLE(\%)} = \frac{\text{weight of loaded drug}}{\text{weight of drug in feed}} \times 100$$

2.6. Pharmacokinetics Studies. The mice were handled under protocols approved by Soochow University Laboratory Animal Center and the Animal Care and Use Committee of Soochow University. Pharmacokinetics studies of PTX-HA-PLGA NPs were performed in nude mice (5 mg PTX/kg, n = 3). Taxol was used as a control. At 0.05, 0.25, 0.5, 1, 2, 4, 8, 12, and 24 h post injection for PTX-HA-PLGA NPs while 0.0333, 0.0833, 0.1667, 0.5, 1, 2, and 4 h post injection for the Taxol group, 20 μL of blood samples were collected in heparinized tubes. Each blood sample was dissolved in 1.0 mL of acetonitrile/methanol (1/1) with brief sonification. After extracting PTX overnight, the resulting dispersion was centrifuged at 13 000 rpm for 20 min, and the supernatant was withdrawn and evaporated to dryness. The residue was redissolved in 250 μL of acetonitrile, and the solution was filtered with a 0.45 μm filter. The amount of PTX was measured by HPLC.

2.7. NIRF Imaging and Biodistribution. To determine the in vivo biodistribution of HA-PLGA NPs, a near-infrared fluorophore Cy5 labeled HA (HA-Cy5) was employed to coat onto PLGA NPs as described above for fluorescence imaging. HA-Cy5 was prepared by the reaction of Cy5-NHS with amino groups of HA-Lys-NH_2 which was obtained as a previous report.[31] Human breast tumor xenografts were established by subcutaneous inoculation of 5 × 10^6 MCF-7 cells in 50 μL of PBS into the right hind flank of each mouse. When the tumor size reached about 200 mm^3, 150 μL of Cy5-labeled HA-PLGA NPs in PBS was intravenously administrated at a concentration of 20 μg/mL. Noninvasive fluorescent imaging at various time intervals from 2 to 48 h after the injection was carried out using the IVIS Lumina II imaging system (Caliper Life Sciences). For ex vivo fluorescence imaging, MCF-7 tumor-bearing mice were sacrificed following 8 h iv injection with Cy5-labeled HA-PLGA NPs. The tumor block and several major organs were collected and imaged using the IVIS Lumina II imaging system.

The in vivo biodistribution of PTX-HA-PLGA NPs was studied in MCF-7 tumor-bearing mice. Eighteen mice with tumor size of ca. 200 mm^3 were randomly assigned to two groups followed by intravenously injection of PTX-HA-PLGA NPs and Taxol, respectively (5 mg PTX/kg). Three mice were sacrificed at 4, 8, and 12 h post injection and the tumor block and several major organs were collected. The samples were homogenized in methanol (2 volumes of tissue) to extract PTX using a homogenizer (IKA T25) at 20 000 rpm for 1 min, 500 μL of acetonitrile was added, and the mixture was placed at −24 °C for 24 h followed by centrifugation. The supernatant was taken, dried, and redissolved in acetonitrile (500 μL) for HPLC measurement.

2.8. In Vivo Antitumor Efficacy. The in vivo antitumor efficacy of PTX−PLGA NPs was assessed using MCF-7 human breast cancer xenografts. Treatments were initiated when tumor size reached 50−80 mm^3. The mice were randomly divided into four groups (n = 6): (i) PTX-HA-PLGA NPs, (ii) Taxol, (iii) bare HA-PLGA NPs, and (iv) PBS (blank control). Different PTX formulations in 0.15 mL of PBS (5 mg PTX/kg) was intravenously administrated on day 0, 3, 6, 9, and 12. Tumor volume was calculated by the formula: $V = 0.5 \times L \times W \times H$, wherein L, W, and H are the tumor dimension at the longest, widest, and highest points, respectively. Relative tumor volumes were calculated as V/V_0 (V_0 is the tumor volume at day 0). Mice were weighed with the relative body weights normalized to their initial weights. Mice were deemed to be dead once the tumor volume reaching 1000 mm^3.

3. RESULTS AND DISCUSSION

3.1. Synthesis of Vitamin E-O(EG_2-Glu). Vitamin E-O(EG_2-Glu) (VEOEG) was obtained by ROP of EG_2-Glu-NCA using vitamin E-NH_2 as an initiator (Scheme 2). Vitamin E-NH_2 was readily synthesized with a yield of 72.9% by coupling ethylenediamine to vitamin E (Scheme 2). ^{1}H NMR demonstrated clear signals owing to both VE (δ 0.83−0.87, 1.07−1.37, 1.52, 1.77, 2.02, 2.08, 2.58) and ethylenediamine moieties (δ 2.90 and 3.33) (Figure S1B). The signals at δ 2.58

Scheme 2. Synthetic Route for Vitamin E-O(EG_2-Glu) (VEOEG)[a]

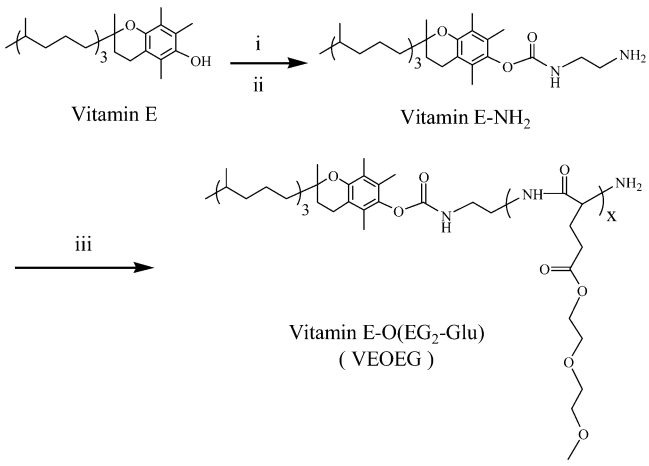

[a]Conditions: (i) 4-nitrophenyl chloroformate, pyridine, DCM, 30 °C, 24 h; (ii) ethylenediamine, pyridine, DCM, 30 °C, 24 h; (iii) EG_2-Glu-NCA, DCM, 25 °C, 12 h.

DOI: 10.1021/acs.biomac.6b00380
Biomacromolecules 2016, 17, 2367−2374

Table 1. Characteristics of Vitamin E-O(EG_2-Glu)

entry	$[M]_0/[I]_0$	DP ^{1}H NMR[a]	M_n (kg/mol) ^{1}H NMR[a]	M_n (kg/mol) GPC[b]	Đ GPC[b]	CMC (mg/L)[c]	HLB[d]
1	6	5.0	1.7	1.6	1.04	189.3	13.8
2	9	8.4	2.4	1.8	1.16	192.6	15.8
3	10	9.2	2.6	1.9	1.14	203.8	16.1

[a]Determined by ^{1}H NMR through comparing the methylene protons of EG_2 at δ 3.68−3.54 with methyl protons of vitamin E at δ 0.87−0.83. [b]Determined by GPC measurements. [c]Determined with pyrene as a fluorescence probe. [d]HLB = 20 × M_h/M_{total}, in which M_h and M_{total} are the molecular weights of the hydrophilic part and whole molecule, respectively.

Table 2. Characteristics of PLGA NPs and HA-PLGA NPs

		PLGA NPs				HA-PLGA NPs			
entry	VEOEG Conc (mg/mL)	size (nm)[a]	PDI[a]	zeta (mV)[b]	VEOEG content (wt %)[c]	size (nm)[a]	PDI[a]	zeta (mV)[b]	HA content (wt %)[d]
1	0.15	157	0.07	25.2	5.78	165	0.05	−29.6	4.92
2	0.30	148	0.04	25.9	6.55	156	0.11	−30.5	5.05
3	0.45	135	0.06	26.6	7.30	143	0.09	−31.0	5.15

[a]Determined by DLS. [b]Measured by electrophoresis at 25 °C in water. [c]Determined by ^{1}H NMR (400 MHz, $CDCl_3$) through comparing the methylene protons of EG_2 at δ 3.68−3.54 with the methine proton of PLGA at δ 5.21. [d]Determined using Cy5 as a fluorescence probe.

and 2.90 had an integral ratio close to 1:1, supporting equivalent coupling of VE and ethylenediamine. The polymerization of EG_2-Glu-NCA was conducted in DCM at 25 °C, similar to previous reports.[32,33] ^{1}H NMR showed characteristic signals of O(EG_2-Glu) block (δ 4.24, 3.68−3.54, 3.40−3.36, 1.99−1.88) and vitamin E end-group (δ 2.07, 2.03, 1.78, 1.53, 1.37−1.07, 0.87−0.83) (Figure 1A). The degree of polymerization (DP) of O(EG_2-Glu) was estimated, through comparing the signals at δ 3.68−3.54 (methylene protons of EG_2, **n**) and δ 0.87−0.83 (vitamin E methyl protons, **a**), to be 5.0, 8.4 and 9.2, which were proportional to the design (Table 1). GPC measurements showed that VEOEG had low polydispersities (PDI < 1.2) (Table 1). MALDI-TOF mass spectrum further confirmed that thus obtained VEOEG had a narrow molecular weight distribution with major peaks corresponding to m/z = 516.4 (VE-NH_2) + n × 231.1 (EG_2-Glu) + 23.0 (Na^+) (Figure 1B). Moreover, the mass spectrum of VEOEG displayed a Poisson distribution centered at the exact molecular weight measured by ^{1}H NMR, further confirming that the polymerization is well-controlled. It should be noted that there exists also a minor mass distribution corresponding to m/z = 516.4 (VE-NH_2) + n × 231.1 (EG_2-Glu) + 112.1 (pyroglutamate) + 23.0 (Na^+), which was due to formation of a cyclic end-group (pyroglutamate) as a result of backbiting reaction and elimination of methyl diglycol.[34] TNBSA assay showed that 66.5% VEOEG contained an amino end group. These VEOEG had a HLB value of 13.8−16.1 (Table 1), indicating that VEOEG could be a good surfactant for O/W emulsification. In addition, VEOEG exhibited a CMC of ca. 200 mg/L (Table 1).

3.2. Preparation of PLGA and HA-PLGA NPs. VEOEG was employed as a novel surfactant for the fabrication of multifunctional PLGA NPs. Notably, DLS measurements showed that thus obtained NPs had small hydrodynamic sizes and extremely low polydispersities (PDI = 0.04−0.07) (Figure S3A). The size of NPs decreased from 157 to 135 nm with increasing VEOEG concentrations from 0.15 to 0.45 mg/mL (Table 2). Mei et al. recently reported that PLGA NPs prepared via nanoprecipitation using TPGS (0.30 mg/mL) had a mean size of ca. 140 nm and a PDI of 0.15.[30,35] TEM micrograph revealed that PLGA NPs possessed a spherical morphology (Figure S3B). As expected, PLGA NPs displayed a positive surface charge of around +25.5 mV, which arises from the terminal amino groups of VEOEG stabilizers located on the surface of NPs. In comparison, PLGA NPs stabilized with PVA and TPGS generally display a negative surface charge.[35,36] XPS measurements corroborated presence of about 3.71% N 1s at the surface of PLGA NPs formed at 0.45 mg/mL VEOEG (Figure S4). ^{1}H NMR showed that VEOEG content on PLGA NPs increased from 5.78 to 7.30 wt % with increasing VEOEG concentrations from 0.15 to 0.45 mg/mL (Table 2). Thus, the resulting PLGA NPs are composed of hydrophobic core for hydrophobic drug encapsulation, and a amphiphilic VEOEG layer on the surface providing stability and functionality.

The presence of amino groups on the surface of PLGA NPs renders them amenable to functionalization with different biomolecules, yielding multifunctional PLGA NPs for tumor-targeting chemotherapy. To demonstrate this, here we coated PLGA NPs with negatively charged HA and further stabilized them by carbodiimide chemistry using EDC/NHS as coupling agents. HA is a natural polysaccharide, and can target to CD44 receptor overexpressing cancer cells like MCF-7 breast cancer cells, A549 human lung tumor cells and LP1 human multiple myeloma cells.[37−40] The results showed that PLGA NPs following coating with HA maintained a small size (143−165 nm) and narrow PDI (0.05−0.11) (Table 2). TEM micrograph confirmed that HA-PLGA NPs had a uniform size distribution (Figure S3B). Importantly, HA-PLGA NPs displayed a negative surface charge of about −30.0 mV, indicating successful coating of PLGA NPs with HA. In order to determine HA content, we labeled HA with Cy5 and quantified HA by fluorescence measurements. The results showed that HA-PLGA NPs contained ca. 5 wt % HA (Table 2). As expected, HA-PLGA NPs were robust against 1000-fold dilution as well as 10% FBS (Figure S3C). These robust multifunctional PLGA NPs could have a great potential in active tumor-targeting delivery of various drugs and proteins.[41−43]

3.3. Loading and in Vitro Drug Release. In the following, we prepared PTX-HA-PLGA NPs and investigated their in vitro release behaviors. The results showed that PTX-HA-PLGA NPs had a small size with a mean size of 164 nm, a PDI of 0.16, and a high drug encapsulation efficiency of 80.1% at 0.45 mg/mL VEOEG (Table 3). TEM micrograph demonstrated that PTX-HA-PLGA NPs maintained a spherical morphology (Figure S5). The in vitro drug release was

DOI: 10.1021/acs.biomac.6b00380
Biomacromolecules 2016, 17, 2367−2374

Table 3. Characteristics of PTX-HA-PLGA NPs (Theoretical DLC = 8 wt %)

entry	VEOEG Conc (mg/mL)	size (nm)[a]	PDI[a]	zeta (mV)[b]	DLC (%)[c]	DLE (%)[c]
1	0.15	183	0.23	−26.9	6.1	74.7
2	0.30	174	0.21	−27.3	6.3	78.2
3	0.45	164	0.16	−27.9	6.4	80.1

[a]Determined by DLS. [b]Measured by electrophoresis at 25 °C in water. [c]Determined by HPLC.

proceeded in the medium containing Tween 80 (0.1%, v/v) to increase the solubility of PTX and maintain the sink conditions for PTX release from HA-PLGA NPs. The results showed that ca. 54.0%, 69.2%, and 79.3% of PTX was released from HA-PLGA NPs in 7 d at pH 7.4, 5.0, and 4.0, respectively (Figure 2). Remarkably, burst PTX release that is often reported for PLGA NPs[44] was absent, confirming that PLGA NPs following HA coating have an excellent stability.

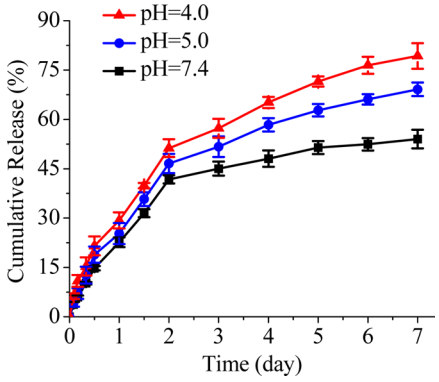

Figure 2. In vitro drug release profiles of PTX-HA-PLGA NPs at pH 7.4, 5.0, and 4.0.

3.4. CD44-Targetability and Antitumor Activity of PTX-HA-PLGA NPs. MTT assays demonstrated that blank HA-PLGA NPs were nontoxic to L929 cells (normal cells) at 350 μg/mL, while displayed moderate cytotoxicity to MCF-7 and U87MG cells (cancerous cells) (Figure 3A). It has been reported that VE derivatives like vitamin E succinate (TOS) and TPGS display selective toxicity to malignant tumor cells.[19,28] Remarkably, PTX- HA-PLGA NPs exhibited slightly higher antitumor effects to CD44 positive MCF-7 cells than Taxol at drug concentrations of 0.01−10 μg/mL (Figure 3B). The IC_{50} of PTX-HA-PLGA NPs in MCF-7 cells was determined to be ca. 0.37 μg PTX equiv./mL, 2-fold lower than Taxol. The pretreatment of MCF-7 cells with free HA resulted in a marked reduction of antitumor activity for PTX-HA-PLGA NPs (Figure 3B), confirming receptor-mediated internalization of HA-PLGA NPs by MCF-7 cells. In contrast, PTX-HA-PLGA NPs showed slightly lower antitumor effect in U87MG cells expressing low level of CD44 receptors than Taxol (Figure 3C). Moreover, PTX-HA-PLGA NPs exhibited a 6.7-fold higher IC_{50} in U87MG cells (2.48 μg PTX equiv/mL) than in MCF-7 cells. It is clear that PTX-HA-PLGA NPs can actively target and efficiently release PTX into CD44 overexpressing cancer cells leading to superb therapeutic activity.

3.5. In Vivo Pharmacokinetics and Biodistribution Studies in MCF-7 Tumor-Bearing Mice. The in vivo pharmacokinetic studies were performed by measuring the

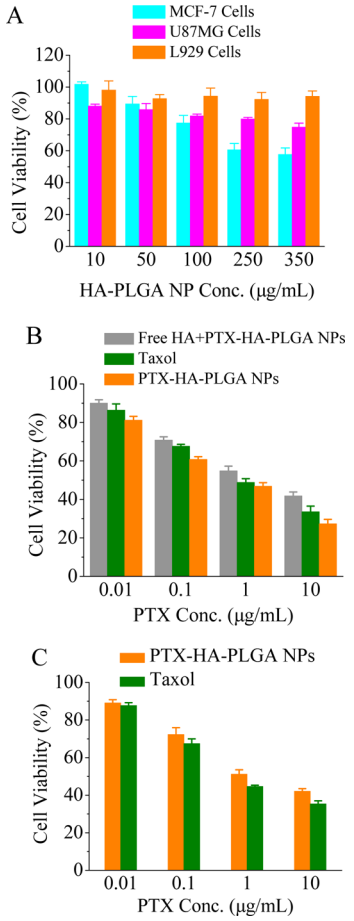

Figure 3. MTT assays. (A) Cytotoxicity of bare HA-PLGA NPs in MCF-7, U87MG, and L929 cells following 48 h incubation; (B,C) Antitumor activity of PTX-HA-PLGA NPs in MCF-7 cells (B), and U87MG cells (C). Cells following 4 h incubation with PTX-HA-PLGA NPs or Taxol were cultured in fresh media for 44 h. For the inhibition experiments, cells were pretreated with free HA (5 mg/mL) for 4 h prior to adding PTX-HA-PLGA NPs. Data are presented as mean ± SD (n = 4, *p < 0.05, **p < 0.01, ***p < 0.001, Student's t test).

plasma PTX levels in mice at predetermined time points after injection of PTX-HA-PLGA NPs (5 mg PTX equiv./kg) using HPLC. Notably, PTX-HA-PLGA NPs revealed a long elimination half-life of 3.14 h, which is significantly improved as compared to Taxol (0.32 h) (Figure 4A).

The in vivo biodistribution of Cy5-labeled HA-PLGA NPs in human MCF-7 tumor-bearing mice was monitored using an IVIS Lumina II imaging system (Caliper Life Sciences). Interestingly, substantial tumor accumulation of HA-PLGA NPs was observed at 2 h post injection and the accumulation in tumor tissue reached the maximum at 8 h (Figure 4B). Strong fluorescence was detected even at 48 h post injection. The ex vivo fluorescence images confirmed that tumor Cy5 fluorescence was stronger than in all the healthy organs (Figure 4C). It should be noted that strong fluorescence was also observed in the liver, which has been reported for most HA nanoparticles due to cellular uptake of phagocytic cells and endothelial cells.[31,45]

Moreover, PTX levels in the healthy organs and tumors following 4, 8, and 12 h injection of PTX-HA-PLGA NPs (5 mg PTX/kg) were quantified by HPLC measurements. The results displayed that PTX-HA-PLGA NPs at 4 h post injection gave a high tumor PTX level of 8.4%ID/g, which was about 6 times

DOI: 10.1021/acs.biomac.6b00380
Biomacromolecules 2016, 17, 2367−2374

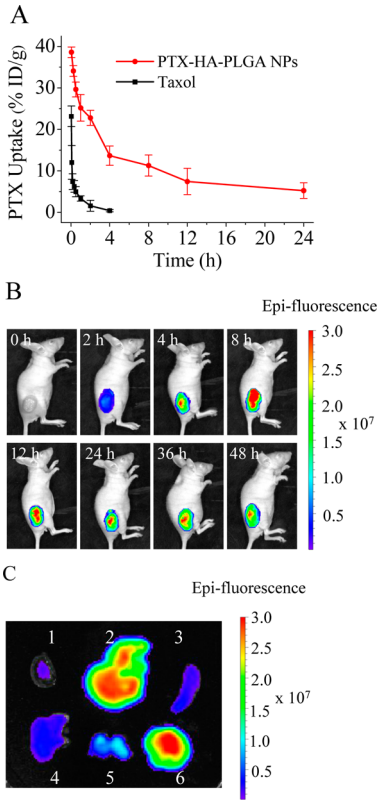

Figure 4. (A) In vivo pharmacokinetics of PTX-HA-PLGA NPs and Taxol in mice (5 mg PTX/kg). (B) Time-dependent in vivo fluorescent images of Cy5-labeled HA-PLGA NPs in MCF-7 tumor bearing mice. (C) NIRF images of the healthy organs and tumor in mice excised at 8 h post injection of Cy5-labeled HA-PLGA NPs (1, heart; 2, liver; 3, spleen; 4, lung; 5, kidney; and 6, tumor).

higher than Taxol (1.4%ID/g). Tumor-to-normal tissue (T/N) distribution ratios showed that PTX-HA-PLGA NPs significantly enhanced tumor selectivity as compared to Taxol (Table S1). All the above results conclude that HA-PLGA NPs can selectively deliver PTX to the breast tumor.

3.6. In Vivo Antitumor Efficacy. The therapeutic performance of PTX-HA-PLGA NPs was investigated using MCF-7 tumor bearing nude mice. The mice were injected with 5 mg PTX equiv./kg on days 0, 3, 6, 9, and 12. Remarkably, tumor growth was almost completely suppressed by PTX-HA-PLGA NPs (Figure 5A). In comparison, continuous tumor progression was witnessed for mice received Taxol, blank HA-PLGA NPs, and PBS, in which the relative tumor volume on day 21 reached 7.7, 12.3, and 16.3, respectively. Figure 5B confirmed that mice following 21 day treatment with PTX-HA-PLGA NPs had the smallest tumor size. Notably, treatment with PTX-HA-PLGA NPs had no influence on mice body weight (Figure 5C), indicating that HA-PLGA NPs had low systemic toxicity. Moreover, survival data revealed that treatment with PTX-HA-PLGA NPs markedly improved the survival time of tumor-bearing mice, in which no death took place within an experimental period of 38 days (Figure 5D). The histological analyses demonstrated that PTX-HA-PLGA NPs generated extensive tumor necrosis without casing significant side effects to the liver and kidney (Figure 6). The low liver damage is surprising as PTX-HA-PLGA NPs were shown to accumulate in the liver. In comparison, Taxol caused significant damage to the liver and kidney. It is evident that

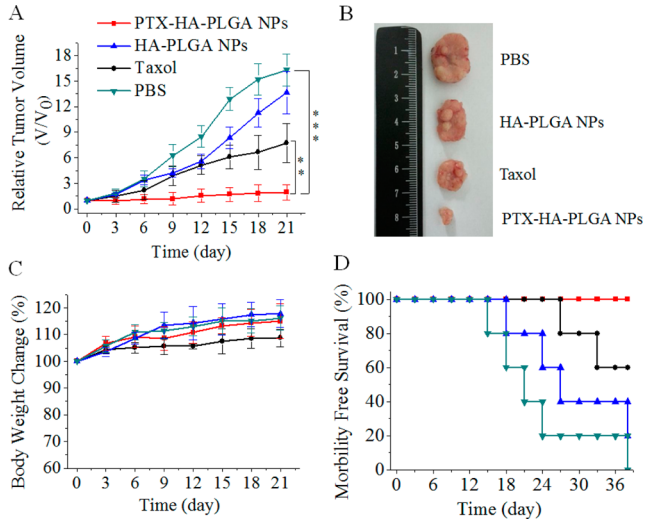

Figure 5. In vivo antitumor activity of PTX-HA-PLGA NPs in MCF-7 tumor-bearing mice. (A) Tumor volume changes of mice. The mice were iv injected with 5 mg PTX equiv/kg on day 0, 3, 6, 9 and 12. (B) Photographs of typical tumor blocks isolated on day 21. (C) Body weight changes within 21 days; and (D) survival curves of mice received different treatments within 21 days. Data are presented as mean ± SD (n = 6). $^{**}p < 0.01$ and $^{***}p < 0.001$ (Student's t test).

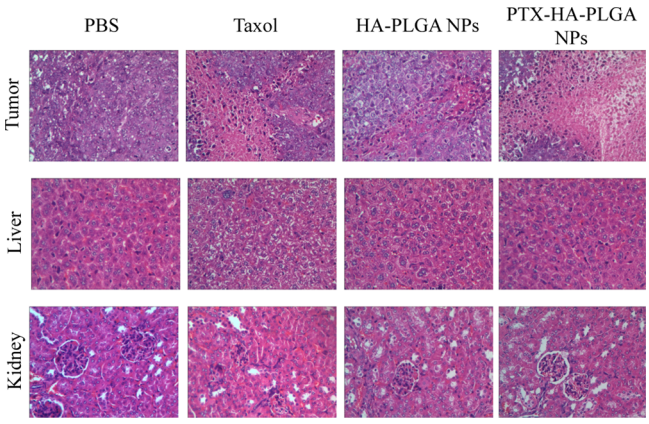

Figure 6. Histological analyses of the tumor, liver, and kidney of mice following 21 day treatment with PTX-HA-PLGA NPs, blank HA-PLGA NPs, Taxol, or PBS. The images were obtained under an Olympus BX41microscope using a 40× objective.

robust PTX-HA-PLGA NPs mediate efficient and targeted delivery of PTX to human breast tumor, resulting in superior therapeutic efficacy with little systemic side effects.

4. CONCLUSIONS

We have shown that amphiphilic vitamin E-oligo(methyl diglycol L-glutamate) (VEOEG) can be easily obtained and applied as a novel biocompatible and functional surfactant for the facile preparation of multifunctional and robust PLGA NPs to achieve targeted, safe, and efficient chemotherapy in vivo. To elaborate our concept, we have coated PLGA NPs with HA (HA-PLGA NPs) and studied their systemic delivery of PTX to CD44 positive breast tumor subcutaneously implanted in the nude mice. Thus, obtained PTX-HA-PLGA NPs exhibit several interesting merits: (i) they show a great stability without burst drug release and with prolonged blood circulation time in vivo; (ii) they show a superb tumor accumulation of 8.4%ID/g; (iii)

DOI: 10.1021/acs.biomac.6b00380
Biomacromolecules 2016, 17, 2367−2374

they demonstrate effective tumor inhibition with little adverse effects; and (iv) VEOEG is biocompatible and biodegradable, and shows selective cytotoxicity to cancerous cells. We are convinced that HA-PLGA NPs with straightforward fabrication, great safety, and excellent targetability to CD44 positive tumor have a great potential for translation to the clinics. This study has shown that, through rational design of functional surfactant, we can obtain multifunctional and robust PLGA nanoparticles for safe and significantly enhanced cancer therapy.

■ ASSOCIATED CONTENT

Supporting Information

The Supporting Information is available free of charge on the ACS Publications website at DOI: 10.1021/acs.biomac.6b00380.

Detailed information on materials and characterization, in vitro drug release, MTT assays, and histological analysis; ^{1}H NMR spectra of vitamin E-4-NC, vitamin E-NH_2, PLGA and VEOEG stabilized PLGA NPs; size distributions of PTX-PLGA NPs and PTX-HA-PLGA NPs; T/N distribution ratios of PTX (PDF)

■ AUTHOR INFORMATION

Corresponding Authors

*Tel./Fax: +86-512-65884933. E-mail: cdeng@suda.edu.cn (C.D.).

*Tel./Fax: +86-512-65880098. E-mail: zyzhong@suda.edu.cn (Z.Z.).

Notes

The authors declare no competing financial interest.

■ ACKNOWLEDGMENTS

This work was supported by the National Natural Science Foundation of China (NSFC 51273137, 51473110, and 51403147) and the National Science Fund for Distinguished Young Scholars (NSFC 51225302).

■ REFERENCES

(1) Hu, C.-M. J.; Fang, R. H.; Wang, K.-C.; Luk, B. T.; Thamphiwatana, S.; Dehaini, D.; Phu, N.; Angsantikul, P.; Wen, C. H.; Kroll, A. V.; Carpenter, C.; Ramesh, M.; Qu, V.; Patel, S. H.; Zhu, J.; Shi, W.; Hofman, F. M.; Chen, T. C.; Gao, W.; Zhang, K.; Chien, S.; Zhang, L. *Nature* **2015**, *526*, 118−121.

(2) Hrkach, J.; Von Hoff, D.; Ali, M. M.; Andrianova, E.; Auer, J.; Campbell, T.; De Witt, D.; Figa, M.; Figueiredo, M.; Horhota, A.; Low, S.; McDonnell, K.; Peeke, E.; Retnarajan, B.; Sabnis, A.; Schnipper, E.; Song, J. J.; Song, Y. H.; Summa, J.; Tompsett, D.; Troiano, G.; Hoven, T. V. G.; Wright, J.; LoRusso, P.; Kantoff, P. W.; Bander, N. H.; Sweeney, C.; Farokhzad, O. C.; Langer, R.; Zale, S. *Sci. Transl. Med.* **2012**, *4*, 128ra39.

(3) Kim, Y.; Lobatto, M. E.; Kawahara, T.; Chung, B. L.; Mieszawska, A. J.; Sanchez-Gaytan, B. L.; Fay, F.; Senders, M. L.; Calcagno, C.; Becraft, J.; Saung, M. T.; Gordon, R. E.; Stroes, E. S. G.; Ma, M.; Farokhzad, O. C.; Fayad, Z. A.; Mulder, W. J. M.; Langer, R. *Proc. Natl. Acad. Sci. U. S. A.* **2014**, *111*, 1078−1083.

(4) Guo, Y.; Wang, D.; Song, Q.; Wu, T.; Zhuang, X.; Bao, Y.; Kong, M.; Qj, Y.; Tan, S.; Zhang, Z. *ACS Nano* **2015**, *9*, 6918−6933.

(5) Danhier, F.; Ansorena, E.; Silva, J. M.; Coco, R.; Le Breton, A.; Preat, V. *J. Controlled Release* **2012**, *161*, 505−522.

(6) Acharya, S.; Sahoo, S. K. *Adv. Drug Delivery Rev.* **2011**, *63*, 170−183.

(7) Mundargi, R. C.; Babu, V. R.; Rangaswamy, V.; Patel, P.; Aminabhavi, T. M. *J. Controlled Release* **2008**, *125*, 193−209.

(8) Vermonden, T.; Censi, R.; Hennink, W. E. *Chem. Rev.* **2012**, *112*, 2853−2888.

(9) Menon, J. U.; Kona, S.; Wadajkar, A. S.; Desai, F.; Vadla, A.; Nguyen, K. T. *J. Biomed. Mater. Res., Part A* **2012**, *100A*, 1998−2005.

(10) Rao, J. P.; Geckeler, K. E. *Prog. Polym. Sci.* **2011**, *36*, 887−913.

(11) Rahimian, S.; Fransen, M. F.; Kleinovink, J. W.; Amidi, M.; Ossendorp, F.; Hennink, W. E. *Biomaterials* **2015**, *61*, 33−40.

(12) Sahoo, S. K.; Panyam, J.; Prabha, S.; Labhasetwar, V. *J. Controlled Release* **2002**, *82*, 105−114.

(13) Zhang, Z.; Tan, S.; Feng, S.-S. *Biomaterials* **2012**, *33*, 4889−4906.

(14) Mu, L.; Feng, S. S. *J. Controlled Release* **2002**, *80*, 129−144.

(15) Mu, L.; Feng, S. S. *Pharm. Res.* **2003**, *20*, 1864−1872.

(16) Zhu, H.; Chen, H.; Zeng, X.; Wang, Z.; Zhang, X.; Wu, Y.; Gao, Y.; Zhang, J.; Liu, K.; Liu, R.; Cai, L.; Mei, L.; Feng, S.-S. *Biomaterials* **2014**, *35*, 2391−2400.

(17) Li, P.-Y.; Lai, P.-S.; Hung, W.-C.; Syu, W.-J. *Biomacromolecules* **2010**, *11*, 2576−2582.

(18) Shen, J.; Yin, Q.; Chen, L.; Zhang, Z.; Li, Y. *Biomaterials* **2012**, *33*, 8613−8624.

(19) Youk, H. J.; Lee, E.; Choi, M. K.; Lee, Y. J.; Chung, J. H.; Kim, S. H.; Lee, C. H.; Lim, S. J. *J. Controlled Release* **2005**, *107*, 43−52.

(20) Nomoto, T.; Fukushima, S.; Kumagai, M.; Machitani, K.; Arnida; Matsumoto, Y.; Oba, M.; Miyata, K.; Osada, K.; Nishiyama, N.; Kataoka, K. *Nat. Commun.* **2014**, *5*, 3545.

(21) Deng, C.; Wu, J.; Cheng, R.; Meng, F.; Klok, H.-A.; Zhong, Z. *Prog. Polym. Sci.* **2014**, *39*, 330−364.

(22) Deming, T. J. *Chem. Rev.* **2016**, *116*, 786−808.

(23) He, C.; Zhuang, X.; Tang, Z.; Tian, H.; Chen, X. *Adv. Healthcare Mater.* **2012**, *1*, 48−78.

(24) Lu, H.; Wang, J.; Song, Z.; Yin, L.; Zhang, Y.; Tang, H.; Tu, C.; Lin, Y.; Cheng, J. *Chem. Commun.* **2014**, *50*, 139−155.

(25) Oliveira, H.; Perez-Andres, E.; Thevenot, J.; Sandre, O.; Berra, E.; Lecommandoux, S. *J. Controlled Release* **2013**, *169*, 165−170.

(26) Wu, L.; Zou, Y.; Deng, C.; Cheng, R.; Meng, F.; Zhong, Z. *Biomaterials* **2013**, *34*, 5262−5272.

(27) Tangsangasaksri, M.; Takemoto, H.; Naito, M.; Maeda, Y.; Sueyoshi, D.; Kim, H. J.; Miura, Y.; Ahn, J.; Azuma, R.; Nishiyama, N.; Miyata, K.; Kataoka, K. *Biomacromolecules* **2016**, *17*, 246−255.

(28) Duhem, N.; Danhier, F.; Preat, V. *J. Controlled Release* **2014**, *182*, 33−44.

(29) Wong, R. S. Y.; Radhakrishnan, A. K. *Nutr. Rev.* **2012**, *70*, 483−490.

(30) Zeng, X.; Tao, W.; Mei, L.; Huang, L.; Tan, C.; Feng, S.-S. *Biomaterials* **2013**, *34*, 6058−6067.

(31) Zhong, Y.; Zhang, J.; Cheng, R.; Deng, C.; Meng, F.; Xie, F.; Zhong, Z. *J. Controlled Release* **2015**, *205*, 144−154.

(32) Chen, C.; Wang, Z.; Li, Z. *Biomacromolecules* **2011**, *12*, 2859−2863.

(33) Liao, Y.; Dong, C.-M. *J. Polym. Sci., Part A: Polym. Chem.* **2012**, *50*, 1834−1843.

(34) Knoop, R. J. I.; Habraken, G. J. M.; Gogibus, N.; Steig, S.; Menzel, H.; Koning, C. E.; Heise, A. *J. Polym. Sci., Part A: Polym. Chem.* **2008**, *46*, 3068−3077.

(35) Tao, W.; Zeng, X.; Liu, T.; Wang, Z.; Xiong, Q.; Ouyang, C.; Huang, L.; Mei, L. *Acta Biomater.* **2013**, *9*, 8910−8920.

(36) Yin Win, K.; Feng, S. S. *Biomaterials* **2005**, *26*, 2713−2722.

(37) Upadhyay, K. K.; Bhatt, A. N.; Mishra, A. K.; Dwarakanath, B. S.; Jain, S.; Schatz, C.; Le Meins, J.-F.; Farooque, A.; Chandraiah, G.; Jain, A. K.; Misra, A.; Lecommandoux, S. *Biomaterials* **2010**, *31*, 2882−2892.

(38) Ganesh, S.; Iyer, A. K.; Gattacceca, F.; Morrissey, D. V.; Amiji, M. M. *J. Controlled Release* **2013**, *172*, 699−706.

(39) Yang, C.; Wang, X.; Yao, X.; Zhang, Y.; Wu, W.; Jiang, X. *J. Controlled Release* **2015**, *205*, 206−217.

(40) Li, J.; Huo, M.; Wang, J.; Zhou, J.; Mohammad, J. M.; Zhang, Y.; Zhu, Q.; Waddad, A. Y.; Zhang, Q. *Biomaterials* **2012**, *33*, 2310−2320.

(41) Steinbach, J. M.; Seo, Y.-E.; Saltzman, W. M. *Acta Biomater.* **2016**, *30*, 49−61.

(42) Arias, J. L.; Unciti-Broceta, J. D.; Maceira, J.; del Castillo, T.; Hernandez-Quero, J.; Magez, S.; Soriano, M.; Garcia-Salcedo, J. A. *J. Controlled Release* **2015**, *197*, 190−198.
(43) Zhong, Y.; Meng, F.; Deng, C.; Zhong, Z. *Biomacromolecules* **2014**, *15*, 1955−1969.
(44) Danhier, F.; Lecouturier, N.; Vroman, B.; Jerome, C.; Marchand-Brynaert, J.; Feron, O.; Preat, V. *J. Controlled Release* **2009**, *133*, 11−17.
(45) Choi, K. Y.; Min, K. H.; Yoon, H. Y.; Kim, K.; Park, J. H.; Kwon, I. C.; Choi, K.; Jeong, S. Y. *Biomaterials* **2011**, *32*, 1880−1889.

DOI: 10.1021/acs.biomac.6b00380
Biomacromolecules 2016, 17, 2367−2374